



Abderahim Belounar · Faïçal Boussem ·
Mohamed Nabil Houhou · Abdelouahab Tati · Lahcene Fortas

Strain-based finite element formulation for the analysis of functionally graded plates

Received: 23 November 2021 / Accepted: 11 April 2022 / Published online: 17 May 2022
© The Author(s), under exclusive licence to Springer-Verlag GmbH Germany, part of Springer Nature 2022

Abstract This work introduces a novel four-node quadrilateral finite element based on the strain approach and the first-order shear deformation theory for static and free vibration responses of functionally graded (FG) material plates. Material properties of the plate are assumed to be graded across the thickness direction by using a simple power law distribution of the volume fractions constituents. The developed element possesses five essential degrees of freedom per node. This element is obtained by the superposition of two strain-based elements where the first is a membrane with two degrees of freedom per node and the second is a Reissner–Mindlin plate that has three degrees of freedom per node. The displacements field of the proposed element which contains higher-order terms is based on assumed strain functions satisfying compatibility equations. The performance of the suggested element is evaluated through several tests and the obtained results are compared with available solutions from the literature. The results of the present element have proved excellent accuracy and efficiency in predicting bending and free vibration of FG plates.

Keywords Assumed strains · Free vibration · Reissner–Mindlin · FGM plate · Finite element

1 Introduction

Functionally graded materials (FGM) are considered as new composite materials first introduced by the Japanese group of scientists [1, 2] where they have often been used in various structural engineering applications, such as aircraft, aerospace, marine. One of the remarkable advantages of FGM is to ensure the continuity of their mechanical and physical characteristics through the thickness and therefore they are introduced to eliminate the stress concentration at the interface of the layers leading to the delamination encountered in the laminated composites.

Research works on the development of advanced numerical methods for the behaviour analysis of functionally graded (FG) plate structures become among the most important research axes in structural mechanics. Nowadays, the finite element method (FEM) has been proved to be a powerful and reliable computational tool for the analysis of FG structures. Several numerical models based on the FEM have been proposed by

A. Belounar (✉)
Department of Civil Engineering, University Center of Tipaza, Tipaza, Algeria
e-mail: belounarab@yahoo.fr

A. Belounar · M. N. Houhou · L. Fortas
NMISSI Laboratory, Faculty of Science and Technology, Biskra University, Biskra, Algeria

F. Boussem
Department of Hydrocarbons and Renewable Energies, Adrar University, Adrar, Algeria

A. Tati
Laboratoire de Génie Energétique Et Matériaux, Biskra University, Biskra, Algeria

many researchers to predict accurately the behaviour of FG structures. Praveen and Reddy [3] used the FEM to investigate the static and dynamic thermo-elastic behaviour of FG plates. In another research work, Reddy [4] presented the finite element formulations based on the third-order shear deformation theory (TSDT) for analysis of FG plates. Based on the first-order shear deformation theory (FSDT), bending, free vibration and mechanical and thermal buckling of FG plates were studied by Nguyen-Xuan et al. [5, 6] and Natarajan et al. [7] using the edge-based smoothed FEM [5], node-based smoothed FEM [6] and cell-based smoothed FEM [7]. Singha et al. [8] used a high precision plate bending finite element based on the FSDT for the nonlinear analysis of FG plates. Various four unknown shear deformation theories were investigated by Thai and Choi [9] using a four-node displacement finite element with ten degrees of freedom per node for the bending and free vibration responses of FG plates with arbitrary boundary conditions. The in-plane displacements were described by the use of Lagrangian linear interpolation functions, whereas the transverse displacement was given by Hermitian cubic interpolation functions. Moita et al. [10] proposed two non-conforming triangular finite element models based on higher-order shear deformation theory for the linear and geometric nonlinear static analysis of FG plate–shell structures. Based on modified FSDT, recently Tati [11] made an attempt to develop a five unknowns high-order shear deformation plate finite element model to study FG plates subjected to sinusoidal or uniformly distributed transversal loads. Both the assumed natural shear strain technique and the concept of the neutral plane were used to avoid any potential locking phenomenon and the membrane-bending coupling. In another work, Tati [12] investigated the behaviour of buckling for FG plates under mechanical and thermal loadings using his finite element model [11]. Sadgui and Tati [13] formulated a finite element with assumed natural shear strains based on trigonometric shear deformation theory and it was successfully applied for both mechanical buckling and free vibration of FG plates.

Finite element formulation based on the strain approach was first introduced by Ashwell and Sabir [14] where a cylindrical shell element was developed in which the displacements field can be derived from assumed strain functions (by integration). The advantages of this approach presented by various elements [15–21] can be cited as easy satisfaction of the convergence criteria, independent functions for the various assumed strain components satisfying the compatibility equations and obtention of higher-order terms in the displacements field without incorporating non-essential degrees of freedom.

The first attempt to apply the strain-based approach to plate bending problems was presented by Belarbi and Charif [22] using a 3D solid finite element. In their work, an eight-node hexahedral element was developed to analyse the static behaviour for thin and thick plate structures. Since this first work, two improved three-dimensional solid plate elements with nine and eight nodes were proposed [23, 24]. For the nine-node element [23], the number of degrees of freedom of the element is reduced from 27 to 24 using the static condensation technique, whereas for the eight-node element [24], its displacements field satisfies the equilibrium equations as an additional condition. To investigate static and free vibration, Messai et al. [25] formulated and implemented in ABAQUS code a nine-node solid plate element. These all strain-based solid plate elements presented above [22–25] contain only the three translational degrees of freedom (u , v , w) per node and they were used with a change in the law of behaviour using the constants of plane stress and a shear correction coefficient.

This approach has been extended for the development of plate bending elements based on the Reissner–Mindlin theory [26–30] where several elements containing three degrees of freedom (w , β_x , β_y) per node were proposed for isotropic plates [26–30]. One of the best initial studies in this field was the formulation of a rectangular plate element by Belounar and Guenfoud [26] for the linear analysis of plates having only regular shapes. In another investigation, Belounar et al. [27] proposed a three-node triangular element that was successfully used for both static and natural vibration of plates. More recently, to study the responses of linear bending, free vibration and buckling of plates, 4-node triangular and quadrilateral elements were developed [28–30]. These elements were proposed to improve the accuracy of the basic strain-based element [26] which suffers from shear locking for very thin plates. It can be seen that all existing strain-based plate elements were established for only isotropic materials and this has motivated the authors to develop a newly assumed strain finite element for the analysis of FG plates.

In the present study, a quadrilateral element based on the strain approach within the framework of the first-order shear deformation theory is developed for the first time to investigate static and free vibration behaviours of FG plates. The elastic material properties of FG plates are considered to vary across the thickness by a power-law distribution of the volume fractions constituents. The present element named **SBQP20** (Strain-Based Quadrilateral Plate with 20 degrees of freedom) has five essential degrees of freedom (u , v , w , β_x , β_y) at each of the four corner nodes and their displacement functions are obtained by the superposition of two strain-based elements. The first is a membrane element named SBRIE (Strain-Based Rectangular In-plane Element) [15] with two degrees of freedom (u , v) per node, whereas the second is a Reissner–Mindlin plate element called

SBQP (Strain-Based Quadrilateral Plate) [28] which contains three degrees of freedom (w, β_x, β_y) per node. The Reissner–Mindlin plate element (SBQP) [28] previously developed by the authors passes the patch test, free of shear locking, and gives good results in static, free vibration and buckling analyses of isotropic plates. Several numerical examples using the present element (SBQP20) are presented to demonstrate its performances for FG plates and the obtained results are compared to existing analytical and numerical solutions given in the literature.

2 Governing equations

2.1 Displacements and strains

For the first-order shear deformation theory, the components of the displacement vector U, V and W in x, y and z directions, respectively, of any point of coordinates (x, y, z) within the plate are expressed in terms of displacements (u, v and w) and rotations (β_x and β_y) of the mid plane [31] as:

$$z = -\frac{h}{2}; E(z) = E_m.$$

$$V(x, y, z) = v(x, y) + z\beta_y(x, y), \tag{1}$$

$$W(x, y, z) = w(x, y),$$

where, u and v are the components of in-plane displacement vector at any point $(x, y, 0)$ in x and y directions, respectively. The transverse displacement $w(x, y)$ is considered to be constant across the thickness of the plate. The rotations around the x - and y -axes are β_y and β_x , respectively.

The in-plane strain $\{\varepsilon\}$ vector can be written as:

$$\{\varepsilon\} = \{\varepsilon^m\} + z\{\kappa\} \quad \{\varepsilon\} = \{\varepsilon_x \ \varepsilon_y \ \gamma_{xy}\}^T. \tag{2}$$

In which $\{\varepsilon^m\}, \{\kappa\}$ are membrane and bending strains vectors, respectively.

$$\{\varepsilon^m\} = \begin{Bmatrix} \varepsilon_x^m \\ \varepsilon_y^m \\ \gamma_{xy}^m \end{Bmatrix} = \begin{Bmatrix} \frac{\partial u}{\partial x} \\ \frac{\partial v}{\partial x} \\ \frac{\partial u}{\partial y} + \frac{\partial v}{\partial x} \end{Bmatrix}; \quad \{\kappa\} = \begin{Bmatrix} \kappa_x \\ \kappa_y \\ \kappa_{xy} \end{Bmatrix} = \begin{Bmatrix} \frac{\partial \beta_x}{\partial x} \\ \frac{\partial \beta_y}{\partial y} \\ \frac{\partial \beta_x}{\partial y} + \frac{\partial \beta_y}{\partial x} \end{Bmatrix}. \tag{3}$$

The transverse shear strain $\{\gamma\}$ vector is given as:

$$\{\gamma\} = \begin{Bmatrix} \gamma_{xz} \\ \gamma_{yz} \end{Bmatrix} = \begin{Bmatrix} \frac{\partial w}{\partial x} + \beta_x \\ \frac{\partial w}{\partial y} + \beta_y \end{Bmatrix}. \tag{4}$$

2.2 Constitutive equations

FGMs are composed of two or more materials in which the material constituent’s volume fractions change continuously through their thickness (Fig. 1). The relations of Young modulus (E) and density (ρ) [4] are given by:

$$E(z) = (E_c - E_m)V_C + E_m,$$

$$\rho(z) = (\rho_c - \rho_m)V_C + \rho_m, \tag{5}$$

where $V_C = (\frac{1}{2} + \frac{z}{h})^n; (n \geq 0)$.

Poisson’s ratio ν is assumed to be constant through the thickness.

where subscripts c and m indicate the material properties of the ceramic and the metal, respectively, n is the volume fraction exponent, and V_C is the volume fraction of the ceramic (Fig. 2).

For the top: $z = \frac{h}{2}; E(z) = E_c.$

For the bottom: $z = -\frac{h}{2}; E(z) = E_m.$

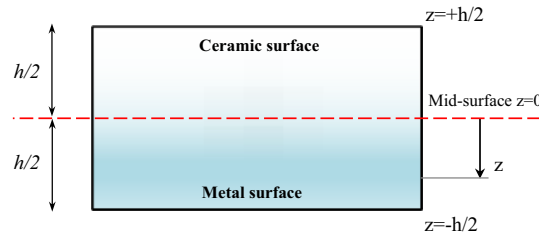


Fig. 1 Functionally graded (FGM) plate geometry

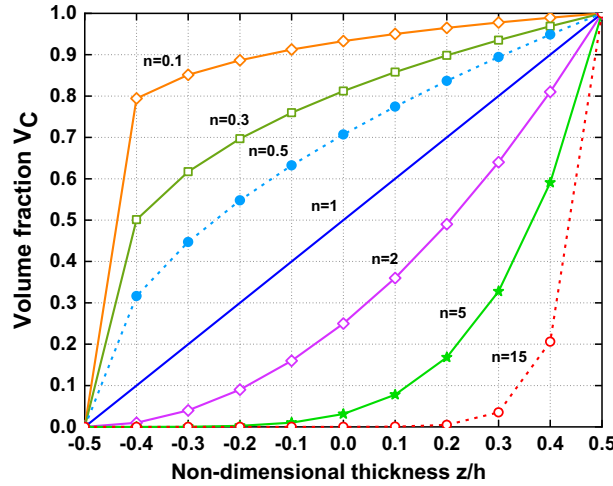


Fig. 2 Variation of the volume fraction function against the non-dimensional thickness

The plate is fully ceramic for n equal to zero, whereas for an infinite value of n , the plate becomes fully metallic.

The constitutive equations of an elastic FGM plate can be given by

$$\{\sigma\} = [H]\{\varepsilon\},$$

$$\begin{Bmatrix} \sigma_x \\ \sigma_y \\ \tau_{xy} \end{Bmatrix} = \begin{bmatrix} H_{11} & H_{12} & 0 \\ H_{12} & H_{22} & 0 \\ 0 & 0 & G_{12} \end{bmatrix} \begin{Bmatrix} \varepsilon_x \\ \varepsilon_y \\ \gamma_{xy} \end{Bmatrix}, \tag{6}$$

$$\{\tau\} = [G]\{\gamma\},$$

$$\begin{Bmatrix} \tau_{xz} \\ \tau_{yz} \end{Bmatrix} = \begin{bmatrix} G_{13} & 0 \\ 0 & G_{23} \end{bmatrix} \begin{Bmatrix} \gamma_{xz} \\ \gamma_{yz} \end{Bmatrix}, \tag{7}$$

$$H_{11} = H_{22} = \frac{E(z)}{1 - \nu^2}; \quad H_{12} = H_{21} = \frac{\nu E(z)}{1 - \nu^2}; \quad G_{12} = G_{13} = G_{23} = \frac{E(z)}{2(1 + \nu)},$$

where stresses and strains are:

$$\{\sigma\} = \{\sigma_x \ \sigma_y \ \tau_{xy}\}^T; \quad \{\varepsilon\} = \{\varepsilon_x \ \varepsilon_y \ \gamma_{xy}\}^T; \quad \{\tau\} = \{\tau_{xz} \ \tau_{yz}\}^T;$$

$$\{\gamma\} = \{\gamma_{xz} \ \gamma_{yz}\}^T.$$

2.3 Stress resultants

The stress resultants are obtained by integration of the stress components σ_x , σ_y , τ_{xy} , τ_{xz} and τ_{yz} through the plate thickness (h) as:

$$\begin{Bmatrix} N_x \\ N_y \\ N_{xy} \end{Bmatrix} = \int_{-h/2}^{h/2} \begin{Bmatrix} \sigma_x \\ \sigma_y \\ \tau_{xy} \end{Bmatrix} dz; \quad \begin{Bmatrix} M_x \\ M_y \\ M_{xy} \end{Bmatrix} = \int_{-h/2}^{h/2} \begin{Bmatrix} \sigma_x \\ \sigma_y \\ \tau_{xy} \end{Bmatrix} z dz; \quad \begin{Bmatrix} T_x \\ T_y \end{Bmatrix} = \int_{-h/2}^{h/2} \begin{Bmatrix} \tau_{xz} \\ \tau_{yz} \end{Bmatrix} dz. \quad (8)$$

By substituting Eqs. (2)–(4), (6) and (7) into Eq. (8), the constitutive equations for axial forces $\{N\}$, bending moments $\{M\}$ and transverse shear forces $\{T\}$ can be obtained as:

$$\{N\} = \begin{Bmatrix} N_x \\ N_y \\ N_{xy} \end{Bmatrix} = [H_m] \begin{Bmatrix} \varepsilon_x^m \\ \varepsilon_y^m \\ \gamma_{xy}^m \end{Bmatrix} + [H_{mb}] \begin{Bmatrix} \kappa_x \\ \kappa_y \\ \kappa_{xy} \end{Bmatrix}, \quad (9)$$

$$\{M\} = \begin{Bmatrix} M_x \\ M_y \\ M_{xy} \end{Bmatrix} = [H_{mb}] \begin{Bmatrix} \varepsilon_x^m \\ \varepsilon_y^m \\ \gamma_{xy}^m \end{Bmatrix} + [H_b] \begin{Bmatrix} \kappa_x \\ \kappa_y \\ \kappa_{xy} \end{Bmatrix}, \quad (10)$$

$$\{T\} = \begin{Bmatrix} T_x \\ T_y \end{Bmatrix} = [H_s] \begin{Bmatrix} \gamma_{xz} \\ \gamma_{yz} \end{Bmatrix}, \quad (11)$$

where the constitutive matrices for membrane $[H_m]$, bending $[H_b]$, coupled membrane-bending $[H_{mb}]$ and shear $[H_s]$ are given by:

$$[H_m] = \int_{-h/2}^{h/2} [H] dz, \quad (12)$$

$$[H_b] = \int_{-h/2}^{h/2} [H] z^2 dz, \quad (13)$$

$$[H_{mb}] = \int_{-h/2}^{h/2} [H] z dz, \quad (14)$$

$$[H_s] = k \int_{-h/2}^{h/2} [G] dz, \quad (15)$$

where k is the shear correction factor.

The earlier Eqs. (9)–(11) can be written in the matrix form as follows:

$$\begin{Bmatrix} N \\ M \\ T \end{Bmatrix} = \begin{bmatrix} [H_m] & [H_{mb}] & 0 \\ [H_{mb}] & [H_b] & 0 \\ 0 & 0 & [H_s] \end{bmatrix} \begin{Bmatrix} \varepsilon^m \\ \kappa \\ \gamma \end{Bmatrix}. \quad (16)$$

3 Finite element formulation of the proposed plate element

The formulated four-node quadrilateral plate element (**SBQP20**) possesses five degrees of freedom per node (Fig. 3) which are three translations (u , v , w) in the x , y and z directions, respectively, and two rotations (β_x , β_y) in the z - y and z - x planes, respectively.

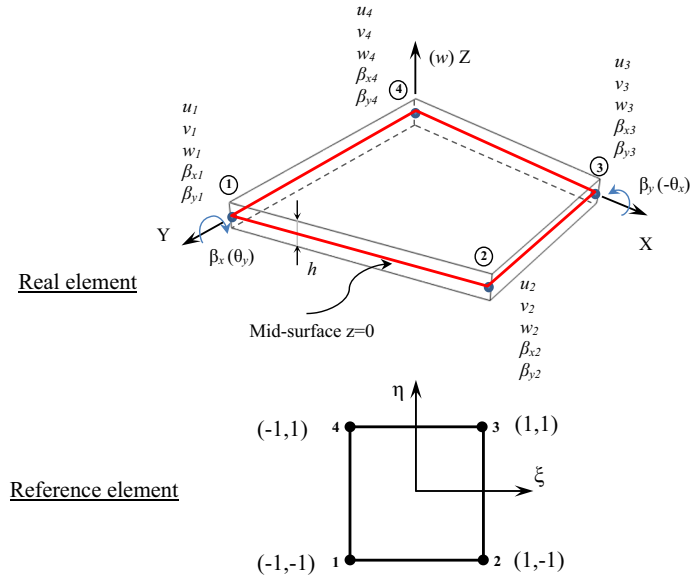


Fig. 3 Quadrilateral FGM plate element (**SBQP20**)

3.1 Displacement interpolation of the SBQP20 element

To formulate the displacement functions of the present element (**SBQP20**), the opportunity is taken to explore the displacements fields obtained from the plate element (SBQP) [28] and the membrane element (SBRIE) [15].

The displacements field given in [15] for the membrane element (SBRIE) is:

$$\begin{Bmatrix} u \\ v \end{Bmatrix} = [P_m]\{\alpha_m\}, \tag{17}$$

where $\{\alpha_m\} = \{\alpha_1, \alpha_2, \dots, \alpha_8\}^T$

$$[P_m] = \begin{bmatrix} 1 & 0 & -y & x & xy & 0 & -\frac{y^2}{2} & \frac{y}{2} \\ 0 & 1 & x & 0 & -\frac{x^2}{2} & y & xy & \frac{x}{2} \end{bmatrix}. \tag{18}$$

For the Reissner–Mindlin plate element (SBQP), the displacement functions [28] are:

$$\begin{Bmatrix} w \\ \beta_x \\ \beta_y \end{Bmatrix} = [P_b]\{\alpha_b\}, \tag{19}$$

where $\{\alpha_b\} = \{\alpha_9, \alpha_{10}, \dots, \alpha_{20}\}^T$

$$[P_b] = \begin{bmatrix} 1 & -x & -y & -\frac{x^2}{2} & -\frac{x^2y}{2} & -\frac{y^2}{2} & -\frac{xy^2}{2} & -\frac{xy}{2} & \frac{x}{2} & \frac{xy}{2} & \frac{y}{2} & \frac{xy}{2} \\ 0 & 1 & 0 & x & xy & 0 & \frac{y^2}{2} & \frac{y}{2} & \frac{1}{2} & \frac{y}{2} & 0 & -\frac{y}{2} \\ 0 & 0 & 1 & 0 & \frac{x^2}{2} & y & xy & \frac{x}{2} & 0 & -\frac{x}{2} & \frac{1}{2} & \frac{x}{2} \end{bmatrix}. \tag{20}$$

The displacements fields of the membrane element Eq. (17) and the Reissner–Mindlin plate element Eq. (19) have been developed using the strain approach where they satisfy the rigid body modes and the constant strains criteria as well as the compatibility equations (“Appendix”).

As stated earlier, the combination of Eqs. (17) and (19) has allowed to have the interpolation functions of the displacement for the formulated plate element (**SBQP20**) as:

$$\{U_c\} = \begin{Bmatrix} u \\ v \\ w \\ \beta_x \\ \beta_y \end{Bmatrix} = \begin{bmatrix} [P_m] & 0 \\ 0 & [P_b] \end{bmatrix} \begin{Bmatrix} \{\alpha_m\} \\ \{\alpha_b\} \end{Bmatrix} = [P]\{\alpha\}, \tag{21}$$

where $\{\alpha\} = \{\{\alpha_m\} \{\alpha_b\}\}^T = \{\alpha_1, \alpha_2, \dots, \alpha_{20}\}^T$.

$$[P] = \begin{bmatrix} [P_m] & 0 \\ 0 & [P_b] \end{bmatrix}. \quad (22)$$

The transformation matrix $[C]$ which relates the element 20 degrees of freedom ($\{q_e\}^T = (u_1, v_1, w_1, \beta_{x1}, \beta_{y1}, \dots, u_4, v_4, w_4, \beta_{x4}, \beta_{y4})$) to the 20 constants ($\{\alpha\}^T = (\alpha_1, \dots, \alpha_{20})$) can be given as:

$$\{q_e\} = [C]\{\alpha\}, \quad (23)$$

where

$$[C] = [[P_1] [P_2] [P_3] [P_4]]^T. \quad (24)$$

And the matrix $[P_i]$ is calculated from Eq. (22) for each of the four element nodes coordinates (x_i, y_i) , ($i = 1, 2, 3, 4$) to obtain:

$$[P]_i = \begin{bmatrix} [P_m]_i & [0] \\ [0] & [P_b]_i \end{bmatrix}_{\text{nodes}, i=1, 2, 3, 4}. \quad (25)$$

Now, we can derive the constant parameters vector $\{\alpha\}$ according to Eq. (23)

$$\{\alpha\} = [C]^{-1}\{q_e\}. \quad (26)$$

Then, substituting Eq. (26) into Eq. (21), we obtain:

$$\{U_e\} = [P][C]^{-1}\{q_e\} = [N]\{q_e\}, \quad (27)$$

where

$$[N] = [P][C]^{-1}. \quad (28)$$

3.2 Evaluation of the strain matrices

For membrane behaviour, the strains $\{\varepsilon^m\}$ are expressed in terms of displacements as:

$$\{\varepsilon^m\} = \begin{Bmatrix} \varepsilon_x^m \\ \varepsilon_y^m \\ \gamma_{xy}^m \end{Bmatrix} = \begin{bmatrix} \partial/\partial x & 0 \\ 0 & \partial/\partial y \\ \partial/\partial y & \partial/\partial x \end{bmatrix} \begin{Bmatrix} u \\ v \end{Bmatrix}. \quad (29)$$

Substitution of Eq. (21) in Eq. (29) yields

$$\{\varepsilon^m\} = \begin{bmatrix} \partial/\partial x & 0 \\ 0 & \partial/\partial y \\ \partial/\partial y & \partial/\partial z \end{bmatrix} [[P_m] [0]]_{2 \times 20} \{\alpha\} = [Q_m]\{\alpha\}. \quad (30)$$

In which the membrane strains matrix $[Q_m]$ is:

$$[Q_m] = \begin{bmatrix} 0 & 0 & 0 & 1 & y & 0 & 0 & 0 & 0 & 0 & 0 & 0 & 0 & 0 & 0 & 0 & 0 & 0 & 0 & 0 \\ 0 & 0 & 0 & 0 & 0 & 1 & x & 0 & 0 & 0 & 0 & 0 & 0 & 0 & 0 & 0 & 0 & 0 & 0 & 0 \\ 0 & 0 & 0 & 0 & 0 & 0 & 0 & 1 & 0 & 0 & 0 & 0 & 0 & 0 & 0 & 0 & 0 & 0 & 0 & 0 \end{bmatrix}. \quad (31)$$

For Reissner–Mindlin plate theory, the curvatures $\{\kappa\}$ and the transverse shear strains $\{\gamma\}$ are given in terms of displacements as:

$$\{\kappa\} = \begin{Bmatrix} \kappa_x \\ \kappa_y \\ \kappa_{xy} \end{Bmatrix} = \begin{bmatrix} 0 & \partial/\partial x & 0 \\ 0 & 0 & \partial/\partial y \\ 0 & \partial/\partial y & \partial/\partial x \end{bmatrix} \begin{Bmatrix} w \\ \beta_x \\ \beta_y \end{Bmatrix}, \quad (32)$$

$$\{\gamma\} = \begin{Bmatrix} \gamma_{xz} \\ \gamma_{yz} \end{Bmatrix} = \begin{bmatrix} \partial/\partial x & 1 & 0 \\ \partial/\partial y & 0 & 1 \end{bmatrix} \begin{Bmatrix} w \\ \beta_x \\ \beta_y \end{Bmatrix}. \quad (33)$$

Substituting Eq. (21) into Eqs. (32) and (33), we have

$$\{\kappa\} = \begin{bmatrix} 0 & \partial/\partial x & 0 \\ 0 & 0 & \partial/\partial y \\ 0 & \partial/\partial y & \partial/\partial x \end{bmatrix} [[0] [P_b]]_{3 \times 20} \{\alpha\} = [Q_b] \{\alpha\}, \tag{34}$$

$$\{\gamma\} = \begin{bmatrix} \partial/\partial x & 1 & 0 \\ \partial/\partial y & 0 & 1 \end{bmatrix} [[0] [P_b]]_{3 \times 20} \{\alpha\} = [Q_s] \{\alpha\}. \tag{35}$$

In which the bending $[Q_b]$ and the transverse shear $[Q_s]$ strains matrices are:

$$[Q_b] = \begin{bmatrix} 0 & 0 & 0 & 0 & 0 & 0 & 0 & 0 & 0 & 0 & 0 & 0 & 0 & 1 & y & 0 & 0 & 0 & 0 & 0 & 0 \\ 0 & 0 & 0 & 0 & 0 & 0 & 0 & 0 & 0 & 0 & 0 & 0 & 0 & 0 & 0 & 1 & x & 0 & 0 & 0 & 0 \\ 0 & 0 & 0 & 0 & 0 & 0 & 0 & 0 & 0 & 0 & 0 & 0 & 0 & 0 & 0 & 0 & (2x) & 0 & (2y) & 1 & 0 & 0 & 0 & 0 \end{bmatrix}, \tag{36}$$

$$[Q_s] = \begin{bmatrix} 0 & 0 & 0 & 0 & 0 & 0 & 0 & 0 & 0 & 0 & 0 & 0 & 0 & 0 & 0 & 0 & 0 & 0 & 0 & 1 & y & 0 & 0 \\ 0 & 1 & x \end{bmatrix}. \tag{37}$$

The relationships between the strains $\{\varepsilon^m\}$, $\{\kappa\}$, $\{\gamma\}$ and the element nodal displacements $\{q_e\}$ are obtained by substituting Eq. (26) into Eqs. (30), (34) and (35) to have:

$$\begin{aligned} \{\varepsilon^m\} &= [Q_m][C]^{-1} \{q_e\} = [B_m] \{q_e\}, \\ \{\kappa\} &= [Q_b][C]^{-1} \{q_e\} = [B_b] \{q_e\}, \\ \{\gamma\} &= [Q_s][C]^{-1} \{q_e\} = [B_s] \{q_e\}, \end{aligned} \tag{38}$$

where $\{\varepsilon^m\}$, $\{\kappa\}$ and $\{\gamma\}$ are the membrane, curvatures and transverse shear strains, respectively, and $[B_m]$, $[B_b]$ and $[B_s]$ are strain matrices which are described as follows:

$$[B_m] = [Q_m][C]^{-1}; \quad [B_b] = [Q_b][C]^{-1}; \quad [B_s] = [Q_s][C]^{-1}. \tag{39}$$

3.3 Derivation of the element matrices and the element load vector

The standard weak form for static analysis can be expressed as:

$$\int_{S_e} \delta \{\varepsilon^m\}^T \{N\} dS + \int_{S_e} \delta \{\kappa\}^T \{M\} dS + \int_{S_e} \delta \{\gamma\}^T \{T\} dS = \int_{S_e} \delta \{U_e\}^T \{f_v\} dS. \tag{40}$$

Insertion of Eqs. (16), (27) and (38) into Eq. (40) yields:

$$\begin{aligned} &\delta \{q_e\}^T \left(\int_{S_e} [B_m]^T [H_m] [B_m] dS \right) \{q_e\} + \delta \{q_e\}^T \left(\int_{S_e} [B_m]^T [H_{mb}] [B_b] dS \right) \{q_e\} \\ &+ \delta \{q_e\}^T \left(\int_{S_e} [B_b]^T [H_{mb}] [B_m] dS \right) \{q_e\} + \delta \{q_e\}^T \left(\int_{S_e} [B_b]^T [H_b] [B_b] dS \right) \{q_e\} \\ &+ \delta \{q_e\}^T \left(\int_{S_e} [B_s]^T [H_s] [B_s] dS \right) \{q_e\} = \delta \{q_e\}^T \left(\int_{S_e} [N]^T \{f_v\} dS \right). \end{aligned} \tag{41}$$

The element stiffness matrix $[K^e]$ is composed of the summation of five matrices as:

$$[K^e] = [K_m^e] + [K_{mb}^e] + [K_{bm}^e] + [K_b^e] + [K_s^e], \tag{42}$$

where $[K_m^e]$ is the membrane part of the stiffness matrix, $[K_{mb}^e]$, $[K_{bm}^e]$ are the coupled membrane-bending components, $[K_b^e]$ is the bending part and $[K_s^e]$ is the shear part and these are given as:

$$[K_m^e] = \int_{S_e} [B_m]^T [H_m] [B_m] dS = [C]^{-T} \left(\int_{S_e} [Q_m]^T [H_m] [Q_m] dS \right) [C]^{-1}, \quad (43)$$

$$[K_{mb}^e] = \int_{S_e} [B_m]^T [H_{mb}] [B_b] dS = [C]^{-T} \left(\int_{S_e} [Q_m]^T [H_{mb}] [Q_b] dS \right) [C]^{-1}, \quad (44)$$

$$[K_{bm}^e] = \int_{S_e} [B_b]^T [H_{mb}] [B_m] dS = [C]^{-T} \left(\int_{S_e} [Q_b]^T [H_{mb}] [Q_m] dS \right) [C]^{-1}, \quad (45)$$

$$[K_b^e] = \int_{S_e} [B_b]^T [H_b] [B_b] dS = [C]^{-T} \left(\int_{S_e} [Q_b]^T [H_b] [Q_b] dS \right) [C]^{-1}, \quad (46)$$

$$[K_s^e] = \int_{S_e} [B_s]^T [H_s] [B_s] dS = [C]^{-T} \left(\int_{S_e} [Q_s]^T [H_s] [Q_s] dS \right) [C]^{-1}. \quad (47)$$

The element nodal equivalent load vector $\{F^e\}$ caused by the distributed transverse load $\{f_v\}$ can be written as:

$$\{F^e\} = \int_{S_e} [N]^T \{f_v\} dS. \quad (48)$$

For the free vibration analysis, a weak form of the principle of virtual work under the assumptions of the FSDT can be expressed as:

$$\int_{S_e} \delta\{\varepsilon^m\}^T \{N\} dS + \int_{S_e} \delta\{\kappa\}^T \{M\} dS + \int_{S_e} \delta\{\gamma\}^T \{T\} dS + \int_{S_e} \delta\{U_e\}^T \{\dot{U}\} dS = 0. \quad (49)$$

Inserting Eqs. (16), (27) and (38) in Eq. (49), we have:

$$\begin{aligned} & \delta\{q_e\}^T \left(\int_{S_e} [B_m]^T [H_m] [B_m] dS \right) \{q_e\} + \delta\{q_e\}^T \left(\int_{S_e} [B_m]^T [H_{mb}] [B_b] dS \right) \{q_e\} \\ & + \delta\{q_e\}^T \left(\int_{S_e} [B_b]^T [H_{mb}] [B_m] dS \right) \{q_e\} + \delta\{q_e\}^T \left(\int_{S_e} [B_b]^T [H_b] [B_b] dS \right) \{q_e\} \\ & + \delta\{q_e\}^T \left(\int_{S_e} [B_s]^T [H_s] [B_s] dS \right) \{q_e\} + \delta\{q_e\}^T \left(\int_{S_e} [N]^T [m] [N] dS \right) \{\ddot{q}_e\} = 0. \end{aligned} \quad (50)$$

The element mass matrix $[M^e]$ can be computed by the following equation:

$$[M^e] = \int_{S_e} [N]^T [m] [N] dS = [C]^{-T} \left(\int_{S_e} [P]^T [m] [P] dS \right) [C]^{-1}. \quad (51)$$

For free vibration, the mass matrix $[m]$ which contains the mass density ρ varying in z direction can be given as:

$$[m] = \begin{bmatrix} I_0 & 0 & 0 & I_1 & 0 \\ 0 & I_0 & 0 & 0 & I_1 \\ 0 & 0 & I_0 & 0 & 0 \\ I_1 & 0 & 0 & I_2 & 0 \\ 0 & I_1 & 0 & 0 & I_2 \end{bmatrix}. \quad (52)$$

where $(I_0, I_1, I_2) = \int_{-\frac{h}{2}}^{\frac{h}{2}} \rho(z) (1, z, z^2) dz$.

Table 1 Material properties

Properties	Aluminium (Al)	Zirconia (ZrO ₂)	Alumina (Al ₂ O ₃)
E (GPa)	70	200	380
ν	0.3	0.3	0.3
ρ (kg/m ³)	2707	5700	3800

The element stiffness $[K^e]$ and mass $[M^e]$ matrices given, respectively, in Eqs. (42) and (51) and the element nodal equivalent load vector $\{F^e\}$ of Eq. (48) are numerically computed using an exact Gauss integration. These matrices and vectors are assembled to obtain the structural stiffness and mass matrices ($[K]$, $[M]$) as well as the structural load vector $\{F\}$.

For static and free vibration analysis, the formulations can be, respectively, written:

$$[K]\{q\} = \{F\}, \quad (53)$$

$$([K] - \omega^2[M])\{q\} = 0, \quad (54)$$

where ω is the natural frequency.

4 Numerical results

In this section, we investigate static and free vibration responses of FG plates using the proposed element and its results are compared with existing analytical and numerical solutions. To show the applicability of the present formulation, a set of examples have been performed for different types of FG plates whose properties, including Young's modulus, Poisson's ratio, and density are listed in Table 1. The shear correction factor considered is $k = 5/6$ and the boundary conditions for an arbitrary edge with clamped and simply supported edge conditions are, respectively:

Clamped (C):

$$u = v = w = \beta_x = \beta_y = 0 \text{ at } x = 0, a \text{ and } y = 0, b.$$

Simply supported (S):

$$v = w = \beta_y = 0 \text{ at } x = 0, a,$$

$$u = w = \beta_x = 0 \text{ at } y = 0, b.$$

4.1 Static analysis

4.1.1 Square plates under uniform and sinusoidal loads

Let us consider an Al/ZrO₂ square plate subjected to a uniform load (Fig. 4) with simply supported (SSSS) and clamped (CCCC) boundary conditions and with various values of gradient index ($n = 0, 0.5, 1, 2$). The plate is modelled with different meshes (Fig. 5) and the obtained results of the non-dimensional central displacement ($W = 100w_c E_m h^3 / 12 q_0 a^4 (1 - \nu^2)$) are presented in Table 2 for thickness-to-side ratio ($a/h = 5$). The results obtained from the present formulation are compared with other approaches available in the literature [5, 6, 32–34] and a very good agreement can be observed. It can be seen that the convergence of the results for the proposed element (**SBQP20**) is quite fast for all meshes.

Shear locking free test is considered for simply supported and clamped Al/ZrO₂ plates subjected to uniform load with varying ratios a/h and power-law index n . Using a mesh of 16×16 , the numerical results of the central deflection ($W = 100w_c E_m h^3 / 12 q_0 a^4 (1 - \nu^2)$) presented in Fig. 6 indicate that the **SBQP20** element is not affected by the length-to-thickness ratio for thin plates.

Next, a simply supported Al/Al₂O₃ square plate subjected to sinusoidal load (Fig. 4) is studied with two thickness-to-side ratios ($a/h = 10$ and 100). Table 3 shows the results of the dimensionless displacement ($W = 10w_c E_c h^3 / q_0 a^4$) of the **SBQP20** element using several meshes (Fig. 5) and with different values of volume fraction exponent ($n = 1, 4, 10$). The results of the present element are compared with those of the first-order shear deformation theory (FSDT) [35], the quasi-3D solutions given by Neves et al. [35–37], Carrera et al. [38] and the analytical solutions from Carrera et al. [39]. It is observed that the results of the present element are in

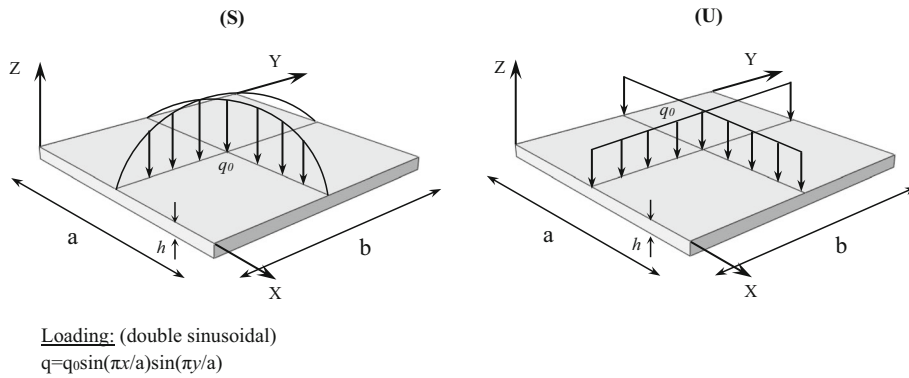


Fig. 4 Square FG plates under sinusoidal load (S) and uniform load (U)

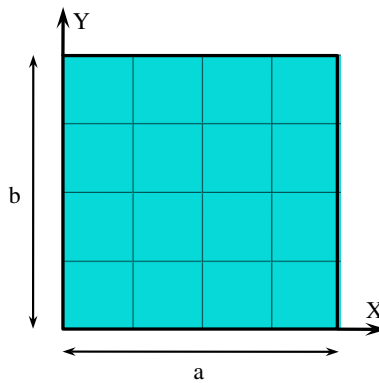


Fig. 5 Square plate with a mesh of $N \times N$ elements

Table 2 Dimensionless deflection (W) of Al/ZrO₂ square plates under uniform loads with ($alh = 5$)

Boundary condition	Methods	n 0	0.5	1	2	
SSSS	SBQP20 (8 × 8)	0.1703	0.2305	0.2696	0.3088	
	SBQP20 (12 × 12)	0.1711	0.2316	0.2709	0.3103	
	SBQP20 (16 × 16)	0.1713	0.2320	0.2714	0.3109	
	SBQP20 (20 × 20)	0.1714	0.2321	0.2716	0.3111	
	SBQP20 (32 × 32)	0.1716	0.2323	0.2718	0.3114	
	IGA-Quadratic [32]	0.1717	0.2324	0.2719	0.3115	
	MITC4 [6]	0.1715	0.2317	0.2704	0.3093	
	ES-DSG3 [5, 6]	0.1700	0.2296	0.2680	0.3066	
	NS-DSG3 [6]	0.1721	0.2326	0.2716	0.3107	
	kip-Ritz [33]	0.1722	0.2403	0.2811	0.3221	
	MLPG [34]	0.1671	0.2505	0.2905	0.3280	
	CCCC	SBQP20 (8 × 8)	0.0750	0.0999	0.1165	0.1349
		SBQP20 (12 × 12)	0.0756	0.1007	0.1175	0.1360
		SBQP20 (16 × 16)	0.0758	0.1010	0.1178	0.1364
SBQP20 (20 × 20)		0.0759	0.1011	0.1180	0.1366	
SBQP20 (32 × 32)		0.0760	0.1012	0.1182	0.1368	
IGA-Quadratic [32]		0.0760	0.1013	0.1183	0.1369	
MITC4 [6]		0.0758	0.1010	0.1179	0.1365	
ES-DSG3 [5, 6]		0.0761	0.1013	0.1183	0.1370	
NS-DSG3 [6]		0.0788	0.1051	0.1227	0.1420	
kip-Ritz [33]		0.0774	0.1034	0.1207	0.1404	
MLPG [34]	0.0731	0.1073	0.1253	0.1444		

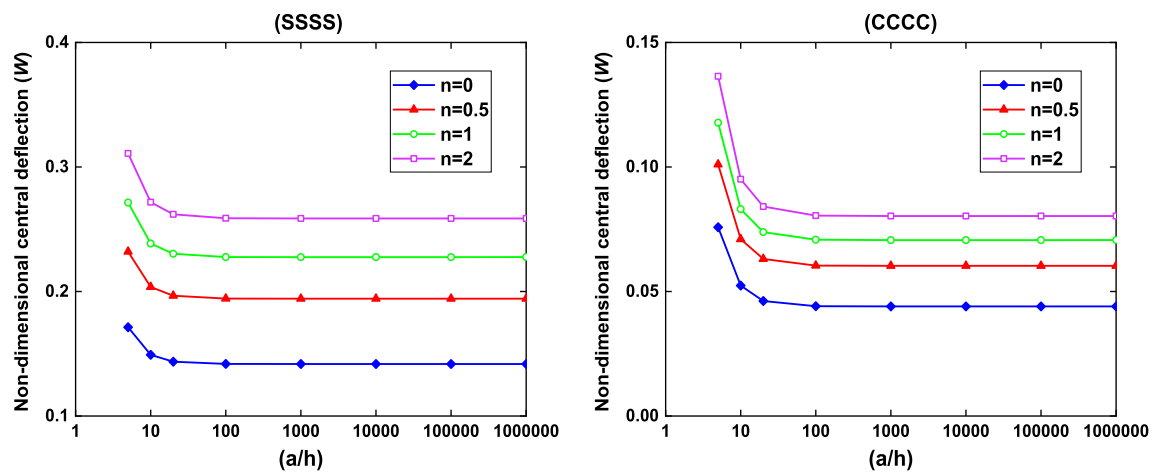


Fig. 6 Dimensionless deflection (W) versus various ratios (a/h) of SSSS and CCCC Al/ZrO₂ square plates under uniform load

Table 3 Dimensionless deflection (W) of SSSS Al/Al₂O₃ square plates under sinusoidal load

a/h	Methods	n		
		1	4	10
10	SBQP20 (8 × 8)	0.5796	0.8591	0.9816
	SBQP20 (12 × 12)	0.5848	0.8672	0.9900
	SBQP20 (16 × 16)	0.5866	0.8700	0.9929
	SBQP20 (20 × 20)	0.5875	0.8713	0.9942
	FSDT [35]	0.5889	0.8736	0.9966
	Quasi-3D [35]	0.5845	0.8750	0.8750
	Quasi-3D [36]	0.5868	0.8698	0.9886
	Quasi-3D [37]	0.5868	0.8700	0.9888
	Quasi-3D [38]	0.5875	0.8821	1.0072
	Reference [39]	0.5875	0.8821	1.0072
100	SBQP20 (8 × 8)	0.5529	0.8135	0.9203
	SBQP20 (12 × 12)	0.5582	0.8219	0.9291
	SBQP20 (16 × 16)	0.5601	0.8248	0.9321
	SBQP20 (20 × 20)	0.5610	0.8262	0.9336
	FSDT [35]	0.5625	0.8280	0.9360
	Quasi-3D [35]	0.5624	0.8286	0.8286
	Quasi-3D [36]	0.5648	0.8241	0.9228
	Quasi-3D [37]	0.5647	0.8240	0.9227
	Quasi-3D [38]	0.5625	0.8286	0.9361
	Reference [39]	0.5625	0.8286	0.9361

good agreement compared with analytical solutions [39] as well as of those the FSDT [35] and the quasi-3D. From Tables 2 and 3, it can be concluded that the non-dimensional central displacement increases with the increase of gradient index n . This can be due to the reduction in stiffness of the structure material caused by an increase in the metallic volume fraction.

4.2 Free vibration analysis

4.2.1 Square plates

The convergence tests of fully simply supported Al/Al₂O₃ square plates (Fig. 5) with three thickness-to-side ratios ($a/h = 5, 10$ and 20) and various values of volume fraction exponent (n) are carried out to examine the stability of the proposed quadrilateral element. Many authors have established this test to investigate the free vibration analysis of FG square plates. Among them, Nguyen-Xuan et al. [5] applied the edge-based smoothed FEM (ES-DSG), the four-node mixed interpolation of tensorial component (MITC4) and the discrete shear gap triangle (DSG3). Matsunaga [40] proposed a higher-order shear deformation theory (HSDT) and Zaho

Table 4 Dimensionless fundamental frequency ($\tilde{\omega}$) of SSSS Al/Al₂O₃ square plate

a/h	Methods	n				
		0	0.5	1	4	10
5	SBQP20 (8×8)	0.21055	0.17991	0.16262	0.13932	0.13198
	SBQP20 (12×12)	0.21091	0.18020	0.16284	0.13946	0.13214
	SBQP20 (16×16)	0.21104	0.18030	0.16292	0.13951	0.13219
	SBQP20 (20×20)	0.21110	0.18035	0.16296	0.13953	0.13222
	ES-DSG (20×20) [5]	0.21218	0.18114	0.16351	0.13992	0.13272
	DSG3 (16×16) [5]	0.21335	0.18216	0.16444	0.14069	0.13343
	MITC4 (16×16) [5]	0.21182	0.18082	0.16323	0.13968	0.13251
	HSDT [40]	0.21210	0.18190	0.16400	0.13830	0.13060
	kip-Ritz [41]	0.20550	0.17570	0.15870	0.13560	0.12840
	Reference [42]	0.21120	0.18050	0.16310	0.13970	0.13240
10	SBQP20 (8×8)	0.05744	0.04878	0.04401	0.03809	0.03641
	SBQP20 (12×12)	0.05758	0.04889	0.04410	0.03815	0.03649
	SBQP20 (16×16)	0.05763	0.04893	0.04413	0.03818	0.03652
	SBQP20 (20×20)	0.05765	0.04895	0.04415	0.03819	0.03653
	ES-DSG (20×20) [5]	0.05800	0.04924	0.04439	0.03839	0.03673
	DSG3 (16×16) [5]	0.05834	0.04954	0.04467	0.03861	0.03693
	MITC4 (16×16) [5]	0.05787	0.04913	0.04429	0.03830	0.03665
	HSDT [40]	0.05777	0.04917	0.04426	0.03811	0.03642
	kip-Ritz [41]	0.05673	0.04818	0.04346	0.03757	0.03591
	Reference [42]	0.05770	0.04900	0.04420	0.03820	0.03660
20	SBQP20 (8×8)	0.01473	0.01248	0.01126	0.00977	0.00937
	SBQP20 (12×12)	0.01477	0.01251	0.01128	0.00979	0.00939
	SBQP20 (16×16)	0.01478	0.01253	0.01129	0.00980	0.00940
	SBQP20 (20×20)	0.01479	0.01253	0.01129	0.00980	0.00941
	ES-DSG (20×20) [5]	0.01488	0.01261	0.01137	0.00986	0.00946
	DSG3 (16×16) [5]	0.01498	0.01270	0.01145	0.00993	0.00952
	MITC4 (16×16) [5]	0.01485	0.01258	0.01134	0.00984	0.00944
	kip-Ritz [41]	0.01464	0.01241	0.01118	0.00970	0.00931
	Reference [42]	0.01480	0.01250	0.01130	0.00980	0.00940

et al. [41] utilized the element-free kip-Ritz method based on the FSDT, whereas Hosseini-Hashemi et al. [42] suggested an analytical approach using FSDT. The results of the fundamental non-dimensional frequency ($\tilde{\omega} = \omega h(\rho_c/E_c)^{1/2}$) of the **SBQP20** element using four meshes (8×8 , 12×12 , 16×16 and 20×20) are presented in Table 4. It can be observed that these results converge towards analytical solutions [42] and agree well with several other available ones [5, 40, 41]. It is also shown (Table 4) that the fundamental natural frequency decreases with the increase in volume fraction exponent n for all cases and this is due to the change in plate rigidity related to the material properties. For a better view, the first normalized frequency ($\tilde{\omega}/\tilde{\omega}_{\text{analytical}}$) is shown in Fig. 7 for three thickness-to-side ratios (a/h) and with different values of the exponent n using a 20×20 mesh and the analytical solution is given by Hosseini-Hashemi et al. [42]. Figure 7 shows that the **SBQP20** element gives better results compared to other methods [5, 40–42] for all cases (a/h).

To verify the accuracy and the performance of the present element to the sensitivity of boundary conditions, two types of FG square plates are considered for several values of power law index (n) and thickness ratio (a/h). The first case of boundary conditions is SSSC and SCSC for Al/Al₂O₃ plate, whereas the second case is SFSC and SFSS for Al/ZrO₂ plate. Tables 5, 6, 7 and 8 illustrate the first non-dimensional frequency ($\tilde{\omega} = \omega a^2(\rho_c/E_c)^{1/2}/h$) of the present element using a 16×16 mesh. The computed results of the **SBQP20** element are compared with analytical solutions based on the FSDT given by Hosseini-Hashemi et al. [42] and other numerical finite element solutions (FEM) based on the polynomial, sinusoidal, hyperbolic, and with FSDT [9]. It can be concluded that the obtained results of the **SBQP20** element are in good agreement with analytical solutions [42], and other available ones based on FEM [9] for all thickness ratios, volume fraction exponent, and boundary conditions.

4.2.2 Circular plate

In this example, a clamped circular FG plate with different thickness-radius ratios (h/R) is considered. The plate consists of Aluminium (Al) at the bottom and Alumina (Al₂O₃) at the top. Using the meshing shown in (Fig. 8), the obtained results of the first six non-dimensional frequencies ($\tilde{\omega} = 100\omega h(\rho_c/E_c)^{1/2}$) of the

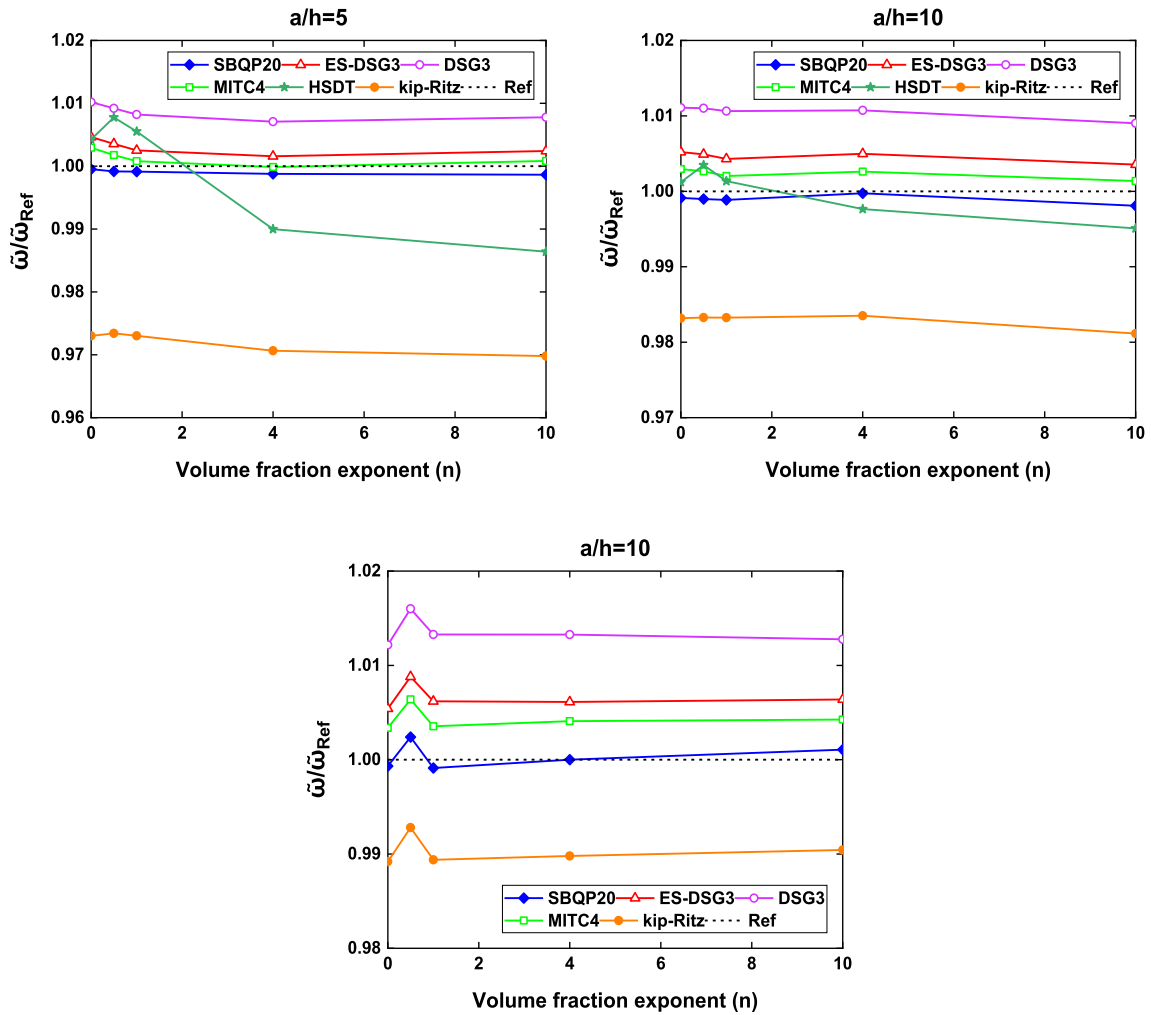


Fig. 7 The normalized frequency ($\tilde{\omega}/\tilde{\omega}_{Ref}$) of SSSS Al/Al₂O₃ plate with various (a/h)

Table 5 Dimensionless fundamental frequency ($\tilde{\omega}$) of SSSC Al/Al₂O₃ square plate

a/h	Methods	n							
		0	0.5	1	2	5	8	10	
5	SBQP20	5.9642	5.1194	4.6361	4.1999	3.8911	3.7736	3.7134	
	FSDT [42]	5.9625	5.1188	4.6356	4.1996	3.8916	3.7746	3.7146	
	FEM (FSDT) [9]	6.0662	5.2038	4.7165	4.2799	3.9755	3.8578	3.7964	
	FEM (poly) [9]	6.0695	5.2145	4.7188	4.2583	3.8945	3.7682	3.7133	
	FEM (sin) [9]	6.0713	5.2135	4.7199	4.2585	3.8916	3.7667	3.7135	
	FEM (sinh) [9]	6.0692	5.3262	4.7185	4.2573	3.8878	3.6163	3.6704	
10	SBQP20	6.7768	5.7655	5.2045	4.7266	4.4457	4.3426	4.2824	
	FSDT [42]	6.7751	5.7649	5.2039	4.7261	4.4462	4.3439	4.2839	
	FEM (FSDT) [9]	6.7739	5.7661	5.2121	4.7415	4.4648	4.3608	4.2994	
	FEM (poly) [9]	6.7742	5.7693	5.2124	4.7333	4.4335	4.3254	4.2665	
	FEM (sin) [9]	6.7745	5.7686	5.2124	4.7330	4.4322	4.3247	4.2662	
	FEM (sinh) [9]	6.7739	5.7927	5.2121	4.7330	4.4326	4.3225	4.2612	
20	SBQP20	7.0541	5.9814	5.3930	4.9024	4.6376	4.5429	4.4836	
	FSDT [42]	7.0526	5.9810	5.3926	4.9019	4.6382	4.5443	4.4854	
	FEM (FSDT) [9]	7.0012	5.9439	5.3683	4.8882	4.6249	4.5271	4.4663	
	FEM (poly) [9]	7.0012	5.9447	5.3683	4.8858	4.6159	4.5170	4.4568	
	FEM (sin) [9]	7.0013	5.9446	5.3684	4.8858	4.6154	4.5166	4.4567	
	FEM (sinh) [9]	7.0012	5.9499	5.3683	4.8858	4.6158	4.5164	4.4556	

Table 6 Dimensionless fundamental frequency ($\tilde{\omega}$) of SCSC Al/Al₂O₃ square plate

a/h	Methods	n						
		0	0.5	1	2	5	8	10
5	SBQP20	6.7785	5.8510	5.3132	4.8116	4.4188	4.2653	4.1910
	FSDT [42]	6.7663	5.8409	5.3039	4.8032	4.4127	4.2604	4.1865
	FEM (FSDT) [9]	6.9897	6.0266	5.4813	4.9797	4.5940	4.4383	4.3607
	FEM (poly) [9]	6.9984	6.0461	5.4873	4.9478	4.4738	4.3077	4.2406
	FEM (sin) [9]	7.0018	6.0452	5.4896	4.9486	4.4701	4.3064	4.2417
	FEM (sinh) [9]	6.9980	6.2609	5.4869	4.9456	4.4577	4.2375	4.0834
10	SBQP20	8.0913	6.9021	6.2382	5.6640	5.3050	5.1700	5.0944
	FSDT [42]	8.0702	6.8847	6.2222	5.6494	5.2930	5.1594	5.0844
	FEM (FSDT) [9]	8.0569	6.8786	6.2338	5.6801	5.3319	5.1940	5.1159
	FEM (poly) [9]	8.0578	6.8843	6.2344	5.6655	5.2794	5.1359	5.0619
	FEM (sin) [9]	8.0587	6.8836	6.2347	5.6655	5.2772	5.1346	5.0615
	FEM (sinh) [9]	8.0578	6.9295	6.2341	5.6652	5.2772	5.1292	5.0486
20	SBQP20	8.5922	7.2917	6.5771	5.9783	5.6479	5.5284	5.4549
	FSDT [42]	8.5674	7.2715	6.5585	5.9612	5.6332	5.5152	5.4423
	FEM (FSDT) [9]	8.4224	7.1647	6.4851	5.9159	5.5895	5.4621	5.3846
	FEM (poly) [9]	8.4224	7.1661	6.4852	5.9116	5.5738	5.4446	5.3683
	FEM (sin) [9]	8.4227	7.1660	6.4853	5.9114	5.5731	5.4441	5.3682
	FEM (sinh) [9]	8.4224	7.1756	6.4851	5.9116	5.5735	5.4433	5.3660

Table 7 Dimensionless fundamental frequency ($\tilde{\omega}$) of SFSC Al/ZrO₂ square plate

a/h	Methods	n						
		0	0.5	1	2	5	8	10
5	SBQP20	3.4463	3.2600	3.1871	3.1714	3.2147	3.2106	3.1986
	FSDT [42]	3.4383	3.2528	3.1804	3.1651	3.2092	3.2055	3.1936
	FEM (FSDT) [9]	3.4863	3.2971	3.2255	3.2134	3.2614	3.2577	3.2452
	FEM (poly) [9]	3.4867	3.2998	3.2259	3.2067	3.2426	3.2397	3.2294
	FEM (sin) [9]	3.4873	3.2996	3.2263	3.2069	3.2422	3.2397	3.2298
	FEM (sinh) [9]	3.4867	3.3204	3.2259	3.2066	3.2417	3.2358	3.2131
10	SBQP20	3.7171	3.5029	3.4234	3.4156	3.4842	3.4857	3.4733
	FSDT [42]	3.7068	3.4936	3.4146	3.4074	3.4766	3.4786	3.4664
	FEM (FSDT) [9]	3.7044	3.4919	3.4152	3.4106	3.4811	3.4823	3.4695
	FEM (poly) [9]	3.7045	3.4927	3.4153	3.4085	3.4750	3.4764	3.4644
	FEM (sin) [9]	3.7045	3.4926	3.4154	3.4085	3.4749	3.4764	3.4645
	FEM (sinh) [9]	3.7044	3.4970	3.4153	3.4084	3.4749	3.4759	3.4635
20	SBQP20	3.8077	3.5835	3.5017	3.4970	3.5752	3.5789	3.5665
	FSDT [42]	3.7962	3.5732	3.4920	3.4877	3.5665	3.5706	3.5584
	FEM (FSDT) [9]	3.7673	3.5476	3.4694	3.4673	3.5450	3.5478	3.5350
	FEM (poly) [9]	3.7673	3.5478	3.4694	3.4668	3.5433	3.5463	3.5337
	FEM (sin) [9]	3.7673	3.5478	3.4694	3.4668	3.5433	3.5463	3.5337
	FEM (sinh) [9]	3.7673	3.5488	3.4694	3.4668	3.5433	3.5463	3.5335

current element are illustrated in Table 9 and the six mode shapes of the circular plate are plotted in Fig. 9. To demonstrate the superiority of the **SBQP20** element, the numerical values of the frequencies are compared with those obtained from FEM with ABAQUS [45], semi-analytical solutions with FSDT [43], uncoupled model (UM) based on the FSDT [44], and HSDT-based IGA [45]. Through the present study, it can be seen that the results of the **SBQP20** element are comparable with analytical and other solutions [43–45]. However, it can be seen that the UM [44] exhibits higher results than the other solutions [43, 45].

5 Conclusion

Based on the FSDT, an efficient four-node quadrilateral element with five degrees of freedom per node, named **SBQP20**, has been formulated for the analysis of FG plates. The proposed element is a combination of a membrane element that possesses two degrees of freedom at each node and a Reissner–Mindlin plate element with three degrees of freedom per node. The displacements fields of the present element that contain higher-

Table 8 Dimensionless fundamental frequency ($\tilde{\omega}$) of SFSS Al/ZrO₂ square plate

a/h	Methods	n						
		0	0.5	1	2	5	8	10
5	SBQP20	3.2445	3.0660	2.9971	2.9842	3.0299	3.0275	3.0164
	FSDT [42]	3.2374	3.0598	2.9912	2.9789	3.0252	3.0231	3.0121
	FEM (FSDT) [9]	3.2504	3.0722	3.0048	2.9943	3.0416	3.0391	3.0278
	FEM (poly) [9]	3.2506	3.0737	3.0051	2.9885	3.0199	3.0240	3.0144
	FEM (sin) [9]	3.2510	3.0741	3.0053	2.9885	3.0255	3.0240	3.0147
	FEM (sinh) [9]	3.2506	3.0897	3.0051	2.9884	3.0252	3.0221	3.0112
10	SBQP20	3.4502	3.2499	3.1759	3.1696	3.2356	3.2377	3.2263
	FSDT [42]	3.4417	3.2424	3.1689	3.1631	3.2297	3.2321	3.2209
	FEM (FSDT) [9]	3.4332	3.2353	3.1636	3.1593	3.2259	3.2275	3.2159
	FEM (poly) [9]	3.4332	3.2358	3.1636	3.1576	3.2208	3.2227	3.2117
	FEM (sin) [9]	3.4333	3.2358	3.1637	3.1576	3.2207	3.2227	3.2118
	FEM (sinh) [9]	3.4332	3.2393	3.1636	3.1575	3.2207	3.2223	3.2110
20	SBQP20	3.5150	3.3076	3.2320	3.2280	3.3009	3.3046	3.2932
	FSDT [42]	3.5058	3.2995	3.2244	3.2208	3.2943	3.2983	3.2871
	FEM (FSDT) [9]	3.4852	3.2815	3.2085	3.2063	3.2787	3.2817	3.2702
	FEM (poly) [9]	3.4852	3.2815	3.2085	3.2057	3.2774	3.2804	3.2689
	FEM (sin) [9]	3.4852	3.2815	3.2085	3.2057	3.2774	3.2804	3.2689
	FEM (sinh) [9]	3.4852	3.2823	3.2085	3.2057	3.2774	3.2804	3.2689

SSSC three sides simply supported and one side clamped, SCSC two sides simply supported and two sides clamped, SFSC two sides simply supported, one side clamped and one free, SFSS three sides simply supported and one free

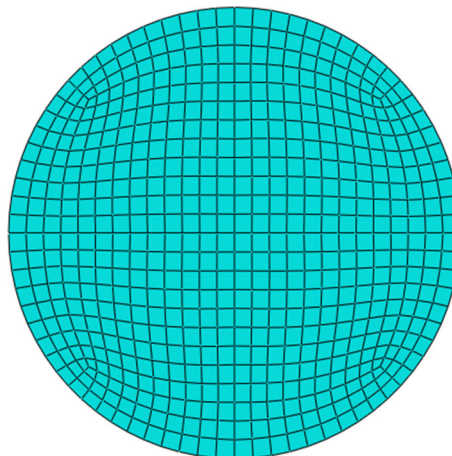


Fig. 8 Meshing of circular plate with 588 quadrilateral elements

Table 9 First six frequencies ($\tilde{\omega}$) of a clamped circular Al/Al₂O₃ plate with ($n = 1$)

h/R	Method	Mode 1	Mode 2	Mode 3	Mode 4	Mode 5	Mode 6
0.01	Semi-analytical [43]	0.0236	0.0491	0.0805	0.0918	0.1178	0.1404
	FEM [45]	0.0234	0.0486	0.0798	0.0909	0.1167	0.1391
	UM [44]	0.0257	0.0535	0.0877	0.1000	0.1283	0.1529
	IGA (HSDT) [45]	0.0236	0.0492	0.0807	0.0924	0.1191	0.1431
	SBQP20	0.0236	0.0493	0.0808	0.0924	0.1196	0.1418
0.1	Semi-analytical [43]	2.3053	4.6934	7.5146	8.5181	10.7128	12.6197
	FEM [45]	2.2888	4.6661	7.4808	8.4829	10.6776	12.5877
	UM [44]	2.5038	5.0831	8.1156	9.1931	11.5376	13.5743
	IGA (HSDT) [45]	2.3076	4.7005	7.5318	8.5380	10.7483	12.6636
	SBQP20	2.3069	4.7052	7.5257	8.5701	10.7868	12.7287
0.2	Semi-analytical [43]	8.6535	16.7666	25.6486	28.7574	34.0756	35.0981
	FEM [45]	8.6403	16.7890	25.7661	28.9152	34.1893	35.3618
	UM [44]	9.3162	17.9164	27.2480	30.4998	–	37.1197
	IGA (HSDT) [45]	8.6787	16.8595	25.8479	29.0092	34.0581	35.4875
	SBQP20	8.6589	16.8050	25.6897	28.9213	34.0909	35.3059

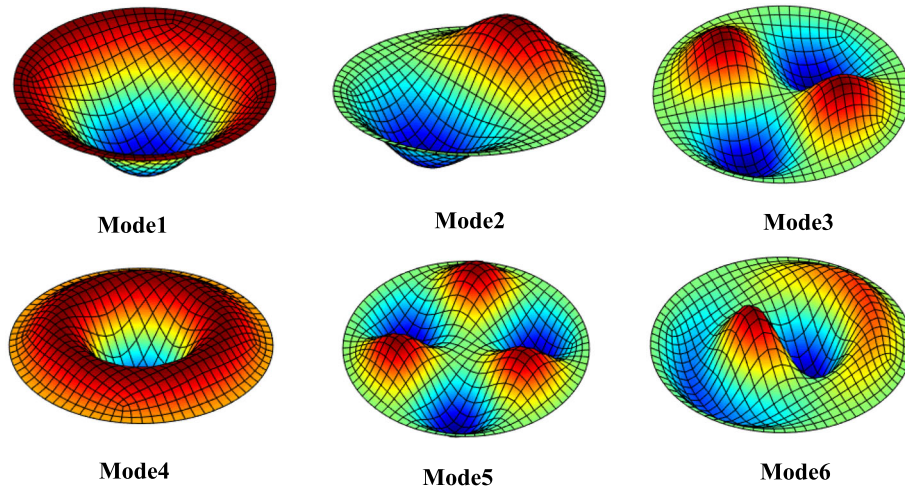


Fig. 9 First six mode shapes of clamped circular Al/Al₂O₃ plate with $h/R = 0.1$

order terms are developed within the framework of the strain approach and they are based on assumed strains satisfying compatibility equations. The accuracy and the reliability of the **SBQP20** element have been proved through several numerical applications for static and free vibration of FG plates with various shapes, boundary conditions, side-to-thickness ratios, and several values of gradient index n . The obtained results of the **SBQP20** element have been found to agree globally well with published reference solutions for both static and free vibration problems. Through this work, the present finite element formulation is thus very promising to provide a simple and effective tool for the computation and simulation of FG plates. In perspective, this element can be further extended for the analysis of FG plates subjected to thermal loads and mechanical/thermal buckling as well as FG shell structures.

Declarations

Conflict of interest On behalf of all authors, the corresponding author states that there is no conflict of interest.

Appendix

For membrane behaviour, the three strains (ϵ_x, ϵ_y and γ_{xy}) given by Eq. (30) satisfy the following compatibility equation

$$\frac{\partial^2 \epsilon_x}{\partial y^2} + \frac{\partial^2 \epsilon_y}{\partial x^2} - \frac{\partial^2 \gamma_{xy}}{\partial x \partial y} = 0. \tag{1a}$$

For Reissner–Mindlin plate theory, the curvatures (κ_x, κ_y and κ_{xy}) and the transverse shear strains (γ_{xz} and γ_{yz}) given in Eqs. (34)–(35) satisfy the following compatibility equations:

$$\begin{aligned} \frac{\partial^2 \kappa_x}{\partial y^2} + \frac{\partial^2 \kappa_y}{\partial x^2} &= \frac{\partial^2 \kappa_{xy}}{\partial x \partial y}; \\ \frac{\partial^2 \gamma_{xz}}{\partial x \partial y} - \frac{\partial^2 \gamma_{yz}}{\partial x^2} + \frac{\partial \kappa_{xy}}{\partial x} &= 2 \frac{\partial \kappa_x}{\partial y}; \\ \frac{\partial^2 \gamma_{yz}}{\partial x \partial y} - \frac{\partial^2 \gamma_{xz}}{\partial y^2} + \frac{\partial \kappa_{xy}}{\partial y} &= 2 \frac{\partial \kappa_y}{\partial x}. \end{aligned} \tag{2a}$$

References

1. Yamanouchi, M., Koizumi, M., Hirai, T., Shiota, I. (eds.): In: Proceedings of 1st International Symposium Functionally Gradient Materials, Japan (1990)
2. Fukui, Y.: Fundamental investigation of functionally gradient material manufacturing system using centrifugal force. *Int. J. Jpn. Soc. Mech. Eng.* **III**(34), 144–148 (1991)
3. Praveen, G.N., Reddy, J.N.: Nonlinear transient thermoelastic analysis of functionally graded ceramic–metal plates. *Int. J. Solids Struct.* **35**(33), 4457–4476 (1998)
4. Reddy, J.N.: Analysis of functionally graded plates. *Int. J. Numer. Methods Eng.* **47**(1–3), 663–684 (2000)
5. Nguyen-Xuan, H., Tran, L.V., Nguyen-Thoi, T., Vu-Do, H.C.: Analysis of functionally graded plates using an edge-based smoothed finite element method. *Compos. Struct.* **93**(11), 3019–3039 (2011)
6. Nguyen-Xuan, H., Tran, L.V., Thai, C.H., Nguyen-Thoi, T.: Analysis of functionally graded plates by an efficient finite element method with node-based strain smoothing. *Thin Walled Struct.* **54**, 1–18 (2012)
7. Natarajan, S., Ferreira, A.J.M., Bordas, S., Carrera, E., Cinefra, M., Zenkour, A.M.: Analysis of functionally graded material plates using triangular elements with cell-based smoothed discrete shear gap method. *Math. Probl. Eng.* (2014). <https://doi.org/10.1155/2014/247932>
8. Singha, M.K., Prakash, T., Ganapathi, M.: Finite element analysis of functionally graded plates under transverse load. *Finite Elem. Anal. Des.* **47**(4), 453–460 (2011)
9. Thai, H.T., Choi, D.H.: Finite element formulation of various four unknown shear deformation theories for functionally graded plates. *Finite Elem. Anal. Des.* **75**(1), 50–61 (2013)
10. Moita, J.S., Correia, V.F., Soares, C.M.M., Herskovits, J.: Higher-order finite element models for the static linear and nonlinear behaviour of functionally graded material plate–shell structures. *Compos. Struct.* **212**(15), 465–475 (2019)
11. Tati, A.: A five unknowns high order shear deformation finite element model for functionally graded plates bending behavior analysis. *J. Braz. Soc. Mech. Sci. Eng.* **43**(1), 1–14 (2021)
12. Tati, A.: Finite element analysis of thermal and mechanical buckling behavior of functionally graded plates. *Arch. Appl. Mech.* **91**, 4571–4587 (2021)
13. Sadgui, A., Tati, A.: A novel trigonometric shear deformation theory for the buckling and free vibration analysis of functionally graded plates. *Mech. Adv. Mater. Struct.* (2021). <https://doi.org/10.1080/15376494.2021.1983679>
14. Ashwell, D.G., Sabir, A.B.: A new cylindrical shell finite element based on simple independent strain functions. *Int. J. Mech. Sci.* **14**(3), 171–183 (1972)
15. Sabir, A.B., Sfeidji, A.: Triangular and rectangular plane elasticity finite elements. *Thin Walled Struct.* **21**(3), 225–232 (1995)
16. Djoudi, M.S., Bahai, H.: A cylindrical strain-based shell element for vibration analysis of shell structures. *Finite Elem. Anal. Des.* **40**(13–14), 1947–1961 (2004)
17. Bouzidi, L., Belounar, L., Guerraiche, K.: Presentation of a new membrane strain-based finite element for static and dynamic analysis. *Int. J. Struct. Eng.* **10**(1), 40–60 (2019)
18. Fortas, L., Belounar, L., Merzouki, T.: Formulation of a new finite element based on assumed strains for membrane structures. *Int. J. Adv. Struct. Eng.* **11**, 9–18 (2019)
19. Khiouani, H.E., Belounar, L., Houhou, M.N.: A new three-dimensional sector element for circular curved structures analysis. *J. Solid Mech.* **12**(1), 165–174 (2020)
20. Belounar, A.: *Eléments finis membranaires et flexionnels à champ de déformation pour l'analyse des structures*. mémoire de Doctorat, Université de Mohamed Khider-Biskra (2019)
21. Boussef, F., Belounar, L.: A plate bending Kirchhoff element based on assumed strain functions. *J. Solid Mech.* **12**(4), 935–952 (2020)
22. Belarbi, M.T., Charif, A.: Développement d'un nouvel élément hexaédrique simple basé sur le modèle en déformation pour l'étude des plaques minces et épaisses. *Rev. eur. élém. finis* **8**(2), 135–157 (1999)
23. Belounar, L., Guerraiche, K.: A new strain based brick element for plate bending. *Alex. Eng. J.* **53**(1), 95–105 (2014)
24. Guerraiche, K., Belounar, L., Bouzidi, L.: A new eight nodes brick finite element based on the strain approach. *J. Solid Mech.* **10**(1), 186–199 (2018)
25. Messai, A., Belounar, L., Merzouki, T.: Static and free vibration of plates with a strain based brick element. *Eur. J. Comput. Mech.* (2019). <https://doi.org/10.1080/17797179.2018.1560845>
26. Belounar, L., Guenfoud, M.: A new rectangular finite element based on the strain approach for plate bending. *Thin Walled Struct.* **43**, 47–63 (2005)
27. Belounar, A., Benmebarek, S., Belounar, L.: Strain based triangular finite element for plate bending analysis. *Mech. Adv. Mater. Struct.* **27**(8), 620–632 (2020)
28. Belounar, A., Benmebarek, S., Houhou, M.N., Belounar, L.: Static, free vibration, and buckling analysis of plates using strain-based Reissner-Mindlin elements. *Int. J. Adv. Struct. Eng.* **11**, 211–230 (2019)
29. Belounar, A., Benmebarek, S., Houhou, M.N., Belounar, L.: Free vibration with Mindlin plate finite element based on the strain approach. *J. Inst. Eng. India C* **101**(2), 331–346 (2020)
30. Boussef, F., Belounar, A., Belounar, L.: Assumed strain finite element for natural frequencies of bending plates. *World J. Eng.* (2021). <https://doi.org/10.1108/WJE-02-2021-0114>
31. Reddy, J.N.: *Mechanics of Laminated Composite Plates and Shells Theory and Analysis*, 2nd edn. CRC Press, New York (2004)
32. Valizadeh, N., Natarajan, S., Gonzalez-Estrada, O.A., Rabczuk, T., Bui, T.Q., Bordas, S.P.A.: NURBS-based finite element analysis of functionally graded plates: static bending, vibration, buckling and flutter. *Compos. Struct.* **99**, 309–326 (2013)
33. Lee, Y.Y., Zhao, X., Liew, K.M.: Thermoelastic analysis of functionally graded plates using the element-free kp-Ritz method. *Smart Mater. Struct.* **18**(3), 1–15 (2009)

34. Gilhooley, D.F., Batra, R.C., Xiao, J.R., McCarthy, M.A., Gillespie, J.W.: Analysis of thick functionally graded plates by using higher-order shear and normal deformable plate theory and MLPG method with radial basis functions. *Comput. Struct.* **80**(4), 539–552 (2007)
35. Neves, A.M.A., Ferreira, A.J.M., Carrera, E., Roque, C.M.C., Cinefra, M., Jorge, R.M.N., Soares, C.M.M.: A quasi-3D sinusoidal shear deformation theory for the static and free vibration analysis of functionally graded plates. *Composites B* **43**(2), 711–725 (2012)
36. Neves, A.M.A., Ferreira, A.J.M., Carrera, E., Cinefra, M., Roque, C.M.C., Jorge, R.M.N., Soares, C.M.M.: A quasi-3D hyperbolic shear deformation theory for the static and free vibration analysis of functionally graded plates. *Compos. Struct.* **94**(5), 1814–1825 (2012)
37. Neves, A.M.A., Ferreira, A.J.M., Carrera, E., Cinefra, M., Roque, C.M.C., Jorge, R.M.N., Soares, C.M.M.: Static, free vibration and buckling analysis of isotropic and sandwich functionally graded plates using a quasi-3D higher-order shear deformation theory and a meshless technique. *Composites B* **44**(1), 657–674 (2013)
38. Carrera, E., Brischetto, S., Cinefra, M., Soave, M.: Effects of thickness stretching in functionally graded plates and shells. *Composites B* **42**(2), 123–133 (2011)
39. Carrera, E., Brischetto, S., Robaldo, A.: Variable kinematic model for the analysis of functionally graded material plates. *AIAA J.* **46**(1), 194–203 (2008)
40. Matsunaga, H.: Free vibration and stability of functionally graded plates according to a 2D higher-order deformation theory. *Compos. Struct.* **82**(4), 499–512 (2008)
41. Zhao, X., Lee, Y.Y., Liew, K.M.: Free vibration analysis of functionally graded plates using the element-free kp-Ritz method. *J. Sound Vib.* **319**(3–5), 918–939 (2009)
42. Hosseini-Hashemi, S., Fadaee, M., Atashipour, S.R.: A new exact analytical approach for free vibration of Reissner-Mindlin functionally graded rectangular plates. *Int. J. Mech. Sci.* **53**(1), 11–22 (2011)
43. Hosseini-Hashemi, S., Fadaee, M., Es'Haghi, M.: A novel approach for in-plane/out-of-plane frequency analysis of functionally graded circular/annular plates. *Int. J. Mech. Sci.* **52**(8), 1025–1035 (2010)
44. Ebrahimi, F., Rastgoo, A., Atai, A.A.: A theoretical analysis of smart moderately thick shear deformable annular functionally graded plate. *Eur. J. Mech. A/Solids* **28**(5), 962–973 (2009)
45. Tran, L.V., Ferreira, A.J.M., Nguyen-Xuan, H.: Isogeometric analysis of functionally graded plates using higher-order shear deformation theory. *Composites B* **51**, 368–383 (2013)